

Extremely rare ultra-fast non-equilibrium processes can be close to equilibrium: RNA unfolding and refolding

Peter Werner and Alexander K. Hartmann

Institut für Physik, Universität Oldenburg, 26111 Oldenburg, Germany

We study numerically the behavior of RNA secondary structures under influence of a varying external force. This allows to measure the work W during the resulting fast unfolding and refolding processes. Here, we investigate a medium-size hairpin structure. Using a sophisticated large-deviation algorithm, we are able to measure work distributions with high precision down to probabilities as small as 10^{-46} . Due to this precision and by comparison with exact free-energy calculations we are able to verify the theorems of Crooks and Jarzynski. Furthermore, we analyze force-extension curves and the configurations of the secondary structures during unfolding and refolding for typical equilibrium processes and non-equilibrium processes, conditioned to selected values of the measured work W , typical and rare ones. We find that the non-equilibrium processes where the work values are close to those which are most relevant for applying Crooks and Jarzynski theorems, respectively, are most and quite similar to the equilibrium processes. Thus, a similarity of equilibrium and non-equilibrium behavior with respect to a mere scalar variable, which occurs with a very small probability but can be generated in a controlled but non-targeted way, is related to a high similarity for the set of configurations sampled along the full dynamical trajectory.

In Statistical Physics, the cleanest and so far best-justified description is obtained for systems in equilibrium. Nevertheless, due to open system boundaries and lack of infinite time to perform experiments or simulations, most real and simulated model systems are constantly in non-equilibrium. A bridge between both worlds is provided. e.g., by the theorems of Jarzynski [1] and Crooks [2], where the distribution $P(W)$ of work W is measured for arbitrary fast non-equilibrium processes obtained from sampling equilibrium initial configurations and possibly stochastic non-equilibrium trajectories. Correspondingly $P_{\text{rev}}(W)$ is the distribution for the reverse process. For a system coupled to a heat bath, Crooks theorem reads $P(W) = P_{\text{rev}}(-W) \exp(-(\Delta F - W)/T)$. This can be used to reconstruct the true free energy difference ΔF between initial and final state, because $P(W)$ and $P_{\text{rev}}(-W)$ cross at $W = \Delta F$. Correspondingly the equation of Jarzynski reads $\langle e^{-W/T} \rangle = e^{-\Delta F/T}$. These and related theorems have lead to many applications and extensions relating equilibrium and non-equilibrium processes [3–10]. A fruitful field of applications is biophysics, where these theorems are used to measure properties of small molecules like RNA.

One major goal of stochastic thermodynamics is to extract equilibrium information from non-equilibrium measurements or simulations [11]. The fluctuation theorems concern specific measurable scalar quantities like work [1, 2, 12], entropy [13–21], or a quantity measuring the volume of the phase space [22]. However, beyond statistics of particular scalar quantities, the fluctuation theorems do not provide information about the unseen equilibrium behavior along the trajectory, i.e., with respect to arbitrary measurable quantities. Standard derivations of the fluctuations theorems only involve terms which include energies and probabilities of the initial and final state. What may we expect when we analyze the full

trajectory of a non-equilibrium process? First, a *typical*, i.e., highly probable sample of a non-equilibrium trajectory will look very different from a corresponding trajectory sampled during an equilibrium process. Second, it is known that when reweighting trajectories suitably in a time-dependent way, they also carry some information about the intermediate not-seen equilibrium states [21, 23, 24] which allows for the reconstruction of full free-energy profiles beyond initial and final state. Third, it is somehow intuitive to believe that the *rare* non-equilibrium processes which contribute most to the estimation of ΔF are in a comprehensive way, without reweighting, similar or even equal to the corresponding equilibrium processes. For the case of the theorems of Crooks and Jarzynski, the statistics of the work distributions are most relevant for particular work values $W = \Delta F$ and $W = W_j^*$, where the latter one is the value where the integrand $e^{-W/T} P(W)$ exhibits a maximum. Note that these values are high improbable to occur for large system sizes. On the other hand, beyond this intuition, there is no solid reason that these rare possibly very fast processes completely resemble true equilibrium processes: A non-equilibrium process always depends on the history, i.e., on many configurations encountered so far, while each equilibrium state in a process does not depend at all on the history. In particular, non-equilibrium processes depend on the speed of performance, while the equilibrium is for infinite low speed.

This question motivates our present work: We investigate in a comprehensive way the dynamics of fast non-equilibrium processes conditioned to various non-equilibrium work values W , typical and rare ones, and compare with the equilibrium process behavior. In particular, we study unfolding and refolding of RNA secondary structures subject to an external force [25]. The former one, denoted as *forward* process, involves stretch-

ing an RNA by subjecting it to an external force f which is increased from starting at zero. For the latter one, denoted as *reverse* process, one starts with a large force and reduces it to zero. For small RNAs consisting of few dozens of bases, Crooks theorem has been confirmed in experiments and simulations [12] for slow unfolding and refolding processes. For such small RNA and slow processes, the resulting work distributions are rather broad and the distribution for forward and reverse processes are close to each other such that they cross at high-probability values which are easily accessible. For larger RNA molecules, the crossing points will move to smaller probabilities, such that the crossing cannot be observed in experiments or standard simulations. To go beyond such limiting system sizes, we applied for our study sophisticated large-deviation algorithms [26, 27], which allowed us to measure probability distributions numerically down to extremely small probabilities. These algorithms have also applied successfully to non-equilibrium processes like the transition-path sampling approach to study protein folding [28, 29], population-based approaches to study asymmetric exclusion processes [30, 31] or Markov-chain Monte Carlo methods to investigate, e.g., traffic models [32] and the Kardar-Parisi-Zhang equation [33]. In particular such an algorithm has also been applied to measure with high precision the work distribution of an Ising model subject to a varying external field [34], providing the first confirmation of the theorems of Jarzynski and Crooks for a large system with many thousands of particles.

Thus, here we will provide similar evidence for RNA secondary structure unfolding and refolding by applying such a rare-event algorithm, allowing us to obtain the work distributions of intermediate-sized RNAs down to probabilities as small as 10^{-46} . Furthermore, we will analyze the temporal structure of the non-equilibrium processes, conditioned to the occurring work values W . We will compare this to the corresponding equilibrium process, which can be sampled exactly [35–37] and efficiently, i.e., in polynomial time, for RNA secondary structures without pseudo-knots. Beyond confirming the theorems of Jarzynski and Crooks we find in particular that the non-equilibrium processes can be very similar in their development to the equilibrium ones. The highest similarity is reached for processes which exhibit a work value W between the values $W = \Delta F$ and $W = W_j^*$ which are most relevant for the Crooks and Jarzynski theorem, respectively.

We will next present our model and the simulation methods we used. Then we show our results and finish by a discussion.

Model — Each RNA molecule is a linear chain of length L of bases from $\{A, C, G, U\}$. A *secondary structure* is a set of pairs of bases, such that only complementary (Watson-Crick) base pairs A-U and C-G are allowed. We forbid *pseudo-knots*, which means that it is always possi-

ble to draw the molecule as a single line and connect all pairs by lines such that no intersections occur.

The energy of an RNA secondary structure consists, first, of the energy from the Watson-Crick pairs, which is its number here for simplicity. Second, the RNA is subject to a force f . This gives rise to an energy contribution $-f \times n$ where n is the *extension* of the structure, i.e., the part of the RNA which is outside the first paired base, plus length 2 for any paired base on the first level. For details see the supplementary material (SM).

Algorithms — For RNA secondary structures it is possible to sample them directly in equilibrium for finite temperatures T in time $O(L^3)$. We used an extension of the approach for the zero-force case [35]. For this purpose, one needs also to calculate partitions functions for some sub sequences, which is possible using *dynamic programming* in polynomial time. These approaches [25, 38] are also extensions of the zero-force case approach [39]. For details see the SM.

For actually performing an unfolding or refolding process, and to measure the performed work W , we started with a configuration \mathcal{S}_0 sampled in equilibrium at initial force $f = f_0$ with $f_0 = 0$ or $f_0 = f_{\max} = 2$. Then the force f was gradually changed in steps Δf up to f_{\max} or down to zero, respectively, while allowing for thermal fluctuations by performing Monte Carlo simulations with creation or removal of pairs as basic moves. Each time the force is changed, we obtained a contribution $\Delta W = -n(\mathcal{S})\Delta f$ to the work, where $n(\mathcal{S})$ is the current extension. For details of the algorithm see the SM.

By repeating an unfolding or refolding simulation many times, one can measure approximately the work distributions $P(W)$ and $P_{\text{rev}}(W)$, respectively. Nevertheless, this *simple sampling approach* allows one only to obtain the work distributions down to rather large probabilities, like 10^{-9} . To obtain the work distributions down to much smaller probabilities, we applied sophisticated large-deviation algorithms [26, 27]. Our approach has already been used to measure work distributions for large Ising systems [34]. The basic idea is to drive the forward and reverse processes, respectively, by vectors ξ of random numbers and control the composition of the vectors with a Markov chain Monte Carlo simulation, with a known, i.e., removable, bias depending on the measured work. For details see the SM.

Results — We considered an RNA sequence which is not too small, such that we were able to observe differences between equilibrium and non-equilibrium secondary structure configurations with suitable resolution. We studied a hairpin structure of length $L = 100$ which has a sequence $(AC)^{25}(UG)^{25}$, resulting in a ground state of one large stack with a small hairpin. For such an RNA size the application of large-deviation algorithm is necessary to measure the work distribution with suitable accuracy such that the theorems of Jarzynski and Crooks can be applied and the unfolding and refolding histories cap-

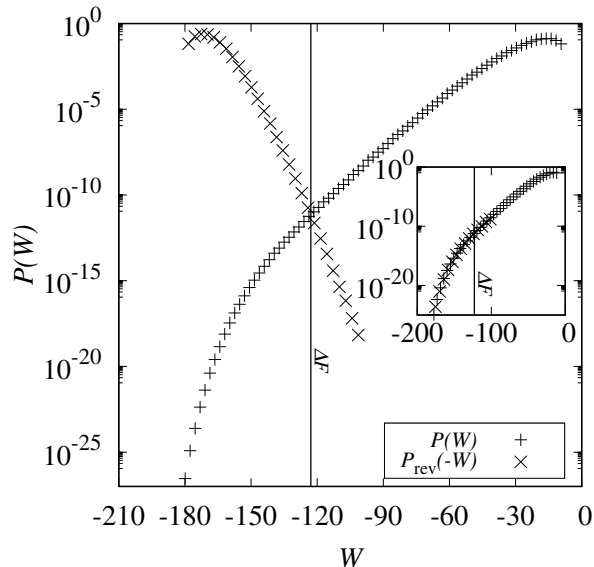


FIG. 1. Plain and mirrored work distributions for $T = 1$ and 8 sweeps of the forward and reverse process, respectively. They intersect near $W = \Delta F$, which is the exact value and indicated by the vertical line. The inset shows the same plot but with the distribution for the reverse process (cross symbols) rescaled as $P_{\text{rev}}(W) \exp(-(\Delta F - W)/T)$, according to the equation of Crooks, yielding a good agreement with $P(W)$.

tured. We considered the RNA coupled to a heat bath at temperatures $T = 0.3$ and $T = 1$, respectively. These are low enough temperatures, such that in the force-free case, the RNA is basically folded, but exhibits thermal fluctuations. Example secondary structures are shown in a figure in the SM. We considered two different speeds of the folding processes, i.e., two different numbers n_{MC} of sweeps performed during the process, here $n_{\text{MC}} = 8$ and $n_{\text{MC}} = 16$. A summary of the simulation parameters is also given in the SM.

In Fig. 1 the work distributions $P(W)$ of the forward and $P_{\text{rev}}(-W)$ of the reverse processes are shown for the case $T = 1$ and $n_{\text{MC}} = 8$. With the application of the large-deviation scheme, we are able to resolve very small probabilities down to 10^{-26} , i.e., over 26 orders in magnitude. The crossing of the distributions at a work value $W = \Delta F$ predicted by the theorem of Crooks [2] can be well observed. For the present model, because we can exactly calculate numerically the partition function, we are able to obtain $\Delta F = 1/T \log\{Z(f = f_0)/Z(f = f_{\text{max}})\}$. Apparently the data matches the expectations from Crooks theorem with high precision.

Crooks relation means that when $P_{\text{rev}}(-W)$ is rescaled according the exponential, it equals $P(W)$. This is also confirmed very convincingly by our data over up to 20 decades, as shown in the inset of Fig. 1. This in partic-

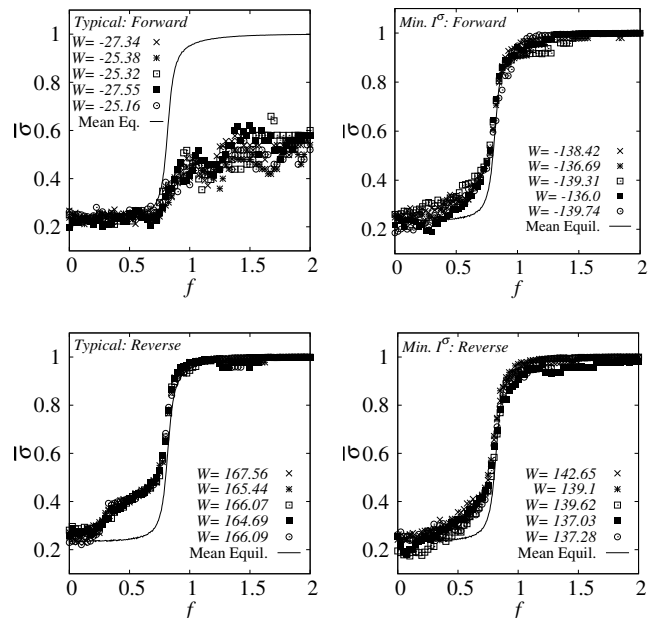


FIG. 2. Average non-equilibrium overlap profiles $\bar{\sigma}(f)$, i.e. between one non-equilibrium and one equilibrium structure, for some sample processes at $T = 1$ and 16 sweeps, with mentioned non-equilibrium work values W . The solid line is the averaged equilibrium overlap, i.e., between two equilibrium structures, respectively. Top row: forward process for typical (left) and very rare (right) values of W . Bottom row: the same for the reverse process. Error bars are smaller than symbol size.

ular shows [34] that our higher-level MCMC simulation is well equilibrated. We obtained similar results for the slower $n_{\text{MC}} = 16$ process. We also studied the lower temperature $T = 0.3$ with $P(W)$ even down to 10^{-46} , see the SM.

Our results allow us to go beyond calculation of distributions and study the actual dynamic processes, conditioned to any value of W . We concentrate now on $T = 1$, the results for $T = 0.3$ are similar. During a forced process, we sampled structures, one for each considered value of f , in equilibrium and in non-equilibrium. To compare two sampled structures we define an *overlap* σ , which runs over all bases of the sequence, and counts $1/L$ if for both structures the base is not paired or if for both structures it is paired with the same base. Otherwise zero is counted, see SM for a formal definition. Overlaps quantities are used frequently to determine order in complex systems, e.g., spin glass [40].

Fig. 2 shows average *non-equilibrium profiles* $\bar{\sigma}(f)$, i.e., averaged overlaps σ as function of f , where in the calculation of the overlaps one structure is a given non-equilibrium sample of a forward or a reverse process and the other structure is a sampled equilibrium structure. Always an average is taken over many equilibrium structures. For comparison in all plots the average *equilibrium*

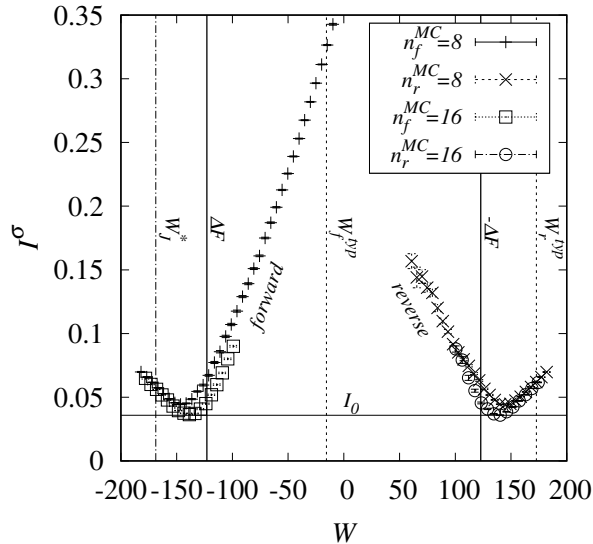


FIG. 3. Integrated difference I^σ between equilibrium and non-equilibrium overlap profiles at $T = 1$, for forward (left) and backward (right) processes. For 16 sweeps the data is only partially shown, for better visibility. The horizontal line indicates I_0 , the value of I^σ in equilibrium. Vertical lines indicate work values at (from left to right) the maximum W_J^* of the Jarzynski integrand, the free energy difference ΔF , the maximum W_f^{typ} of the forward process work distribution, the negative free energy difference $-\Delta F$ and the maximum point W_r^{typ} of the reverse process work distribution.

profile is shown, where both structures are sampled from equilibrium. Our results show that folded structures at low force value f are characterized by a variety of secondary structures, while at high values of f , where the RNA is basically stretched, the secondary structures are very similar to each other. We see that for *typical* work values, i.e., where $P(W)$ and $P_{rev}(W)$ peak, in particular for the forward process, large differences for non-equilibrium profiles compared to the average equilibrium profile occur. For work values near $W = \Delta F \approx -123$ on the other hand, we observe a high similarity, i.e., these very rare non-equilibrium processes enroll close to the equilibrium ones.

We quantify the similarity I^σ of the non-equilibrium processes to the equilibrium case by integrating over all force values f the absolute difference of $\bar{\sigma}(f)$ between the equilibrium and non-equilibrium case, and average this integral over close-by values of W , i.e., obtaining $I^\sigma(W)$. The result is shown in Fig. 3. We observe rather larger differences for typical values of W , while near $W \approx \pm\Delta F$ the similarity is of the order of the similarity I_0 obtained by averaging I^σ over many independent equilibrium processes, which represents the equilibrium fluctuations. Also the forward processes sampled

for work values near the value $W_J^* \approx -170$ where the Jarzynski integrand $P(W)e^{-W/T}$ peaks (see SM) exhibit a high similarity to the equilibrium case. Note that for the reverse process, the value of W_J^* occurs outside our sampled region, thus we do not have processes for this case. For the slower case of $n_{MC} = 16$ sweeps, i.e., a bit nearer to equilibrium, the location minimum moves closer to ΔF and even decreases in height towards the equilibrium value I_0 .

Thus, our results show that the rare processes near $W = \pm\Delta F$ do not only have similar work values like the equilibrium processes, they exhibit also very similar sequences, as function of the force f , of sampled structures. We obtained a similar result when considering force-extension curves, see SM.

Discussion — We studied RNA unfolding and refolding in equilibrium and in non-equilibrium. For the non-equilibrium case, by using sophisticated large-deviation algorithms, we could access a large range of the support of the probability distribution for the work. This allowed us to confirm the theorems of Crooks and Jarzynski over several dozens decades in probability. Furthermore, we analyzed the trajectories in force-extension as well as in secondary-structure space conditioned to various values of W . We observe that near the most relevant, but very improbable, values of W , the sampled trajectories reach a high similarity with true equilibrium. Thus, the study here does not depend on assigning a time-dependent weight to the trajectories, the selection is solely by the total work performed during the process and suitably evaluating fluctuation theorems. Also no other particular similarity to equilibrium is enforced explicitly by our procedure. Our approach and results may open a pathway to learning not only about equilibrium characteristic scalar numbers from non-equilibrium measurements, but even investigating near equilibrium dynamics by performing very fast but biased non-equilibrium simulations. We anticipate that similar studies are feasible and useful for many different types of systems.

For further studies, one could also extend the approach, by storing the configurations of the close-to-equilibrium $W \approx \Delta F$ generated rare trajectories. Starting with these configurations one could perform additional equilibrium simulations at fixed force values, i.e., without performing work, in the hope to get quickly close or even up to equilibrium. We have run some test simulations which show that one can indeed get even much closer to the equilibrium behavior by applying these additional equilibration, apparently perfectly with respect to the force-extension curves, but this also depends on the temperature. Here more studies are needed, in particular a comparison of how good one can equilibrate by just using secondary-structure MC simulations when starting with empty configurations. Also it would be very interesting to see how these results depend of the actual RNA sequence and the corresponding energy landscape.

The simulations were performed at the the HPC cluster CARL, located at the University of Oldenburg (Germany) and funded by the DFG through its Major Research Instrumentation Program (INST 184/157-1 FUGG) and the Ministry of Science and Culture (MWK) of the Lower Saxony State.

SUPPLEMENTARY MATERIAL

RNA secondary structure model

Each RNA molecule is a linear chain $\mathcal{R} = (r_i)_{i=1,\dots,L}$ of bases, also called residues, with $r_i \in \{A, C, G, U\}$ and L is the length of the sequence. For a given sequence \mathcal{R} of bases the secondary structure can be described by a set \mathcal{S} of pairs (i, j) (with the convention $1 \leq i < j \leq L$), meaning that bases r_i and r_j are paired. For convenience, we also use $s(i) = j$ if i is paired to j , which implies $s(j) = i$, and $s(i) = 0$ if i is not paired. We only allow Watson-Crick base pairs. These are formed by hydrogen bonds between *complementary* pairs of bases, i.e., A-U and C-G. Formally, this means for A-U either $r_i = A$ and $r_j = U$ or vice versa, correspondingly for the C-G pair. Two restrictions are used: (i) We exclude so called *pseudo-knots*, that means, for any $(i, j), (i', j') \in \mathcal{S}$, either $i < j < i' < j'$ or $i < i' < j' < j$ must hold, i.e., we follow the notion of pseudo knots being more an element of the tertiary structure [41]. (ii) Between two paired bases a minimum distance is required: $|j - i| > s$ is required, granting some flexibility of the molecule (here $s = 2$).

Every secondary structure \mathcal{S} is assigned a certain energy $E(\mathcal{S})$, we do not explicitly indicate the dependence on the sequence \mathcal{R} . This energy is defined by assigning each pair (i, j) a certain energy $e(r_i, r_j)$ depending only on the kind of bases.

Furthermore there is a contribution arising from the external force f which stretches the chain to its extension $n(\mathcal{S})$, as introduced previously [25]. Thus, $n(\mathcal{S})$ is composed of a length of two units for each globule in the chain plus the number of bases in the free part, i.e., outside any globule. This is illustrated in Fig. 4.

The total energy is the sum over all pairs plus the interaction with the external force

$$E(\mathcal{S}) = \sum_{(i,j) \in \mathcal{S}} e(r_i, r_j) - n(\mathcal{S}) f. \quad (1)$$

By choosing $e(r, r') = +\infty$ for non-complementary bases r, r' pairings of this kind are suppressed. Here we use the most simple energy model, i.e., $e(r, r') = -1$ for complementary bases A-U and C-G.

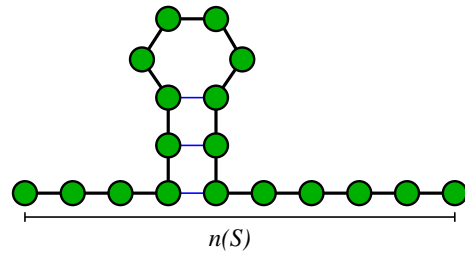


FIG. 4. (color online) An example for a RNA secondary structure with one globule and a line indicating the extension $n(\mathcal{S})$ of the folded RNA. Circles denote bases, thick black lines links between consecutive bases, and thin blue lines hydrogen bonds between complementary bases.

Calculation of partition functions

The partition function $Z_{i,j}$ ($i \leq j$) for sub sequence $r_i \dots r_j$ at inverse temperature $\beta = 1/T$ without external force and without length constraints, obeying the minimum distance s between two paired bases, is given by

$$\begin{aligned} Z_{i,j} &= 1 \quad \text{for } j - i \leq s \\ Z_{i,j} &= Z_{i,j-1} \\ &+ \sum_{k=i}^{j-s-1} Z_{i,k-1} e^{-\beta e(r_k, r_j)} Z_{k+1, j-1} \quad \text{else} \end{aligned} \quad (2)$$

All $O(L^2)$ values of $Z_{i,j}$ can be conveniently calculated [39] by a *dynamic programming approach*, i.e. starting with $Z_{i,i}$ and continuing with increasing values of $j - i$. Since most contributions involve a sum of $O(L)$ terms, the algorithm has a running time of $O(L^3)$.

In order to include the interaction with the external force, one needs additionally the partition function $Q_{1,j,n}$ of the sub sequence $r_1 \dots r_j$ such that the extension is fixed to the value n , with $n \leq j$. We include the fixed index 1 for matching with the notation for $Z_{i,j}$,

Our approach follows the lines of a corresponding methods [25, 38] for calculation of partition functions and ground state energies of RNA secondary structures subject to an external force. The partition function reads :

$$\begin{aligned} Q_{1,1,1} &= 1 \\ Q_{1,j,1} &= 0 \quad \text{for } j > 1, \\ Q_{1,2,2} &= Z_{1,2} \\ Q_{1,j,2} &= 0 \quad \text{for } 2 < j \leq s + 1 \\ Q_{1,j,2} &= e^{-\beta e(r_1, r_j)} Z_{2, j-1} \quad \text{for } j > s + 1 \\ Q_{1,j,n} &= Q_{1, j-1, n-1} + \sum_{k=n-1}^{j-s-1} Q_{1, k-1, n-2} e^{-\beta e(r_k, r_j)} Z_{k+1, j-1}. \end{aligned} \quad (3)$$

Also all these partition functions can be conveniently calculated by dynamic programming in time $O(L^3)$.

This allows us to calculate the partition function with force for sub sequence r_1, \dots, r_j by

$$\tilde{Z}_{1,j}(f) = \sum_{n=1}^j Q_{1,j,n} e^{\beta n f}. \quad (4)$$

Note that the case $n = 0$ can not occur and the case $n = 1$ corresponds only to one single base.

Sampling secondary structures

The availability of the above partition functions allows us to sample secondary structures in the presence of an external force directly, i.e. rejection free, also in polynomial time. The approach is an extension of the zero-force algorithm [35] to the case $f \geq 0$.

For sampling a structure, the following probabilities are needed. The probability $p_{i,j,k}^p$ that for sub sequence r_i, \dots, r_j , without the presence or influence of a force, base j is paired to base k with $i \leq k < j$ and $j - k > s$ is given by

$$p_{i,j,k}^p = \frac{Z_{i,k-1} e^{-\beta e(r_k, r_j)} Z_{k+1, j-1}}{Z_{i,j}}. \quad (5)$$

For $j - k \leq s$, this probability is zero. The probability that base j is not paired is given by

$$p_{i,j}^u = \frac{Z_{i, j-1}}{Z_{i,j}}. \quad (6)$$

The probability $\tilde{p}_{1,j,k}^p(f)$ that for sub sequence r_1, \dots, r_j , with the presence of a force f , base j is paired to base k with $1 \leq k < j$ and $j - k > s$ is given by

$$\tilde{p}_{1,j,k}^p(f) = \frac{\tilde{Z}_{1,k-1}(f) e^{-\beta e(r_k, r_j) + \beta 2f} Z_{k+1, j-1}}{\tilde{Z}_{1,j}(f)} \quad (7)$$

For $j - k \leq s$, this probability is zero. The probability that base j is not paired is given by

$$\tilde{p}_{1,j}^u(f) = \frac{\tilde{Z}_{1, j-1}(f) e^{\beta f}}{\tilde{Z}_{1,j}(f)}. \quad (8)$$

The sampling of a structure is now performed as follows. Each time one starts for the full sequence r_1, \dots, r_L by considering the *case with force* f :

- *Case with force* f for sub sequence r_1, \dots, r_j

Base j is paired to one of the bases $k = 1, \dots, j - s - 1$ with probability $\tilde{p}_{1,j,k}^p(f)$, respectively, and remains unpaired with probability $\tilde{p}_{1,j}^u(f)$.

Now, if base j has been paired to base k , recursively the sequence r_1, \dots, r_{k-1} is treated in the same way (*case with force* f) and the sub sequence r_{k+1}, \dots, r_{j-1} is treated as described in the *case without force*.

If base j has not been paired, the sequence r_1, \dots, r_{j-1} is treated in the same way (*case with force* f).

- *Case without force* for sub sequence r_i, \dots, r_j

Base j is paired to one of the bases $k = i, \dots, j - s - 1$ with probability $p_{i,j,k}^p$, respectively, and remains unpaired with probability $p_{i,j}^u$.

Now, if base j has been paired to base k , recursively the sequence r_i, \dots, r_{k-1} and r_{k+1}, \dots, r_{j-1} are treated in the same way (*case without force*).

If base j has not been paired, the sequence r_1, \dots, r_{j-1} is treated in the same way (*case without force*).

In this way, each time a structure is independently drawn according to the Boltzmann distribution, i.e., the algorithm constitutes ideal sampling.

Folding and Unfolding Algorithm

The algorithm to determine the work for a given sequence \mathcal{R} works as follows: First, a secondary structure is drawn in equilibrium at some given initial value f_0 of the force and for RNA temperature T . Then a Monte Carlo (MC) simulation allowing to change the secondary structure with total of n_{MC} sweeps is performed while the force parameter f is increased or reduced depending on Δf . One sweep consist of $L^2/2$ Monte Carlo steps. During the MC simulation, n_{force} times the force is increased by Δf . For the individual MC steps, each time two random residues i and j are selected. If these are already paired to each other, the pair is removed, i.e., the bond broken, with the usual Metropolis probability $p_{\text{Metr}} = \min\{1, \exp(-\beta \Delta E)\}$ determined by the energy change $\Delta E = -e(r_i, r_j)$. Note that we use negative pair energies, thus we have always $p_{\text{Metr}} = \exp(\beta e(r_i, r_j))$. In case of two non-bonded bases, they will be paired if they are complementary, and if they have a distance larger than s , and if no pseudo-knots would be created. The configuration is not changed when just one of the selected bases is already bounded, since a base can only connect to a single other one. The random numbers which are used during the MC simulation are generated before a call to the subroutine and stored in a vector ξ . In this way, all the randomness is removed outside this subroutine [42], for a reason we will present in the next section. Note that all other parameters like \mathcal{R} , T etc. remain the same during a simulation, thus the work obtained during a unfolding or refolding is a deterministic function of ξ :

algorithm $W(\xi)$
begin
 draw for \mathcal{R} an equilibrium structure \mathcal{S} at
 initial force f_0 and RNA temperature T
 $f = f_0$
 $W = 0$
for $j = 0, \dots, n_{\text{force}}$
begin
 perform $L^2 n_{\text{MC}} / (2n_{\text{force}})$ MC-Steps:
begin
 select two random residues $l, m \in \{1, \dots, L\}$
if $(l, m) \in \mathcal{S}$, remove pair with prob. p_{Metr} .
else if (l, m) is allowed set $\mathcal{S} = \mathcal{S} \cup \{(l, m)\}$
end
 $f = f + \Delta f$
 $W = W - n(\mathcal{S})\Delta f$
end
return(W)
end

The vector $\xi = (\xi_1, \xi_2, \dots, \xi_K)$ contains $K = L - 1 + 3L^2 n_{\text{MC}} / 2$ random numbers which are uniformly distributed in $[0, 1]$. These are all random numbers that are needed to perform one full unfolding or refolding simulation. Each random number has a specific fixed purpose. The first $L - 1$ entries are required to sample an configuration from the partition function, where an individual random number is utilized to determine if base $j \in [2, \dots, L]$ is either connected to base $k \in [1, \dots, j - s - 1]$ or unconnected. Not all these $L - 1$ random numbers are necessarily used during a specific sampling process, e.g., if for base j the remaining sub sequence for a potential pairing partner is too small. In this case, the corresponding random number is just ignored, The subsequent MC steps need three random numbers each, two for selecting a pair and potentially one more, if the Metropolis criterion is used. If not, the third random number is also ignored, respectively. This results in a number of $3L^2 n_{\text{MC}} / 2$ additional entries in ξ .

Note that more efficient Monte Carlo algorithms for RNA secondary structures exists [43, 44], which are event-driven Gillespie algorithms. Also they take as possible Monte Carlo moves only allowed moves into account, i.e., either pairs are removed, or only allowed pairs are proposed, avoiding non-complementary base pairs or pseudo knots. This requires keeping track of the allowed moves, which also generates quite some overhead in computation and it also involves the calculation of necessary corrections factors due to the varying number of accessible neighboring secondary structure configurations, in order to guarantee detailed balance. Also, the Gillespie nature of these algorithms make the use of random numbers dependent on the history of previous events. Nevertheless, for the present application, the work process is embedded into another higher-level Monte-Carlo simula-

tion, see below. For a good performance of the higher-level MC simulation this requires that for each entry of the vector a specific purpose is assigned, as presented above. if this requirement is met, small changes to ξ yield typically small, i.e., not too “chaotic” changes in the resulting work $W = W(\xi)$. This is the case with the present algorithm.

Large-deviation approach

Now we explain how the work simulations can be performed, such that also the tails of the work distribution $P(W)$ with potentially very small probabilities can be obtained. The method has been introduced for the Ising model [34], where more details are given. Here we review only the general idea and present the specific details for our study.

As mentioned in the previous section, for a given sequence \mathcal{R} , temperature T and the other parameters, which are all kept fixed for a set of simulations, the outcome of the unfolding or refolding process is solely determined by the random values contained in the vector ξ . Thus, to perform a standard *simple sampling* simulation, one could each time draw a random vector ξ with each entry being a pseudo random number uniformly distributed in $[0, 1]$. This results in one work value W which sampled from the true distribution. Thus, if one repeats the simple sampling many times, one can collect many work values and calculate a histogram to approximate the full distribution. Nevertheless, running the simple sampling K times, will one only allow to resolve probabilities larger or equal $1/K$ in the histogram.

In order to access to work distribution down to very small probabilities, we did the following: We used a Markov chain Monte Carlo (MCMC) simulation where the states of the simulation are represented by samples $\xi^{(t)}$ of the random vectors used to drive the RNA unfolding or folding simulations. Thus, each state of the Markov chain corresponds to exactly one instance of a full process consisting of starting with an initial state in equilibrium and performing a, typically fast, non-equilibrium process during which the force is changed, the system has a bit of time to relax between two force changes, and a work value $W = W(\xi^{(t)})$ is obtained in the end. Therefore, the MCMC simulation takes place on a higher level than the unfolding or refolding simulations. Now, the main idea is to include a bias in the MCMC simulation, which involves a Metropolis acceptance depending on the change in the resulting work.

To be more precise, say we have the current state $\xi^{(t)}$ with work $W^{(t)} = W(\xi^{(t)})$ in the MCMC simulation. First, we generate a *trial state* ξ' , which we obtain by copying $\xi^{(t)}$ and then redrawing a number $n_\xi < K$ of randomly selected entries from the K entries of $\xi^{(t)}$. Next, we perform a complete work process for ξ' , which results

in the measured work $W' = W(\xi')$. Now, the trial state is accepted, i.e., $\xi^{(t+1)} = \xi'$ with Metropolis probability $\tilde{p}_{\text{Metr}} = \min\{1, \exp(-\Delta W/\Theta)\}$, where $\Delta W = W' - W^{(t)}$ is the change in work and Θ is a temperature-like control parameter. Otherwise, the trial state is rejected, i.e., $\xi^{(t+1)} = \xi^{(t)}$. Note we aim at an empirical acceptance rate around 0.5 such that n_ξ is typically small for small values of Θ and larger for larger values of Θ . Actual values are given below.

Since the setup of the MCMC simulation is like any standard MCMC approach for a system coupled to a heat bath, only that we have replaced the energy by the work and use Θ for the temperature, it is obvious that our approach will sample the true work distribution but including a bias which is exactly the Boltzmann factor $\sim \exp(-W/\Theta)$. As usual, one has to discard the initial phase of the Markov chain, i.e., the equilibration phase, and to draw sample values only at suitable large time intervals. Thus, one can in principle perform simulations for a given value of Θ , measure a histogram approximating the biased distribution $P_\Theta(W) \sim P(W) \exp(-W/\Theta)$, and obtain an estimate, up to the normalization constant, for the true distribution $P(W)$ by multiplication with $\exp(+W/\Theta)$. Note that, technically, to obtain the distribution over a large range of the support, one needs to perform simulations at several suitably chosen values of the control temperature Θ , obtain the normalization constants for all measured histograms and combine them into one single finally normalized histogram [26]. Details, in particular for the case of the work distribution of an Ising model in an external field, can be found elsewhere [34]. This approach has already been applied to other non-equilibrium processes like the Kardar-Parisi-Zhang model [33] or traffic flows [32].

Example secondary structures

In Fig. 5 equilibrium secondary structures are shown. It becomes apparent how the extension increases with the force parameter f .

Simulation parameters

For all unfolding and refolding processes, the force was increased from $f_0 = 0$ to $f_{\text{max}} = 2$ and vice versa, with 400 steps each. Thus, the change of the force was $\Delta f = \pm 0.005$. Table I shows the other simulation parameters we have used.

Work distributions

In Fig. 6 the work distributions for $T = 1$ of the slower process, at total of 16 MC sweeps per process, are shown.

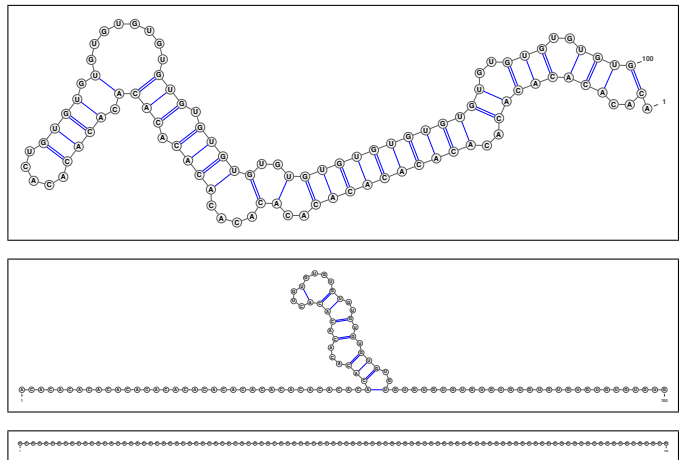


FIG. 5. Exemplary equilibrium secondary structures at $T = 1$ for different forces. Top: $f = 0$. Middle: $f = 0.805$. Bottom: $f = 2$. Drawn with the VARNA package [45].

T	n_{MC}	f	n_Θ	Θ_{min}	Θ_{max}	$n_{\xi,\text{min}}$	$n_{\xi,\text{max}}$	$t_{\text{id}}/10^8$
0.3	8	$0 \rightarrow 2$	17	0.6	7	938	9×10^4	5.44
0.3	8	$2 \rightarrow 0$	10	0.4	2	1587	6×10^4	4.05
0.3	16	$0 \rightarrow 2$	18	0.6	8	1407	12×10^4	2.50
0.3	16	$2 \rightarrow 0$	10	0.4	2	2500	9×10^4	1.82
1	8	$0 \rightarrow 2$	11	0.8	10	354	6×10^4	6.95
1	8	$2 \rightarrow 0$	13	1	5	1350	6×10^4	2.81
1	16	$0 \rightarrow 2$	11	0.8	10	938	75×10^2	4.41
1	16	$2 \rightarrow 0$	10	0.8	5	2344	12×10^4	2.35

TABLE I. Simulation parameters for different temperatures T and for different process speeds n_{MC} and unfolding ($f = 0 \rightarrow 2$) and refolding ($f = 2 \rightarrow 0$) processes. For the large-deviation MCMC simulation n_Θ different values of the temperature-like parameter $\Theta \in [\Theta_{\text{min}}, \Theta_{\text{max}}]$ were considered. In each MCMC step a number $n_\xi \in [n_{\xi,\text{min}}, n_{\xi,\text{max}}]$ of entries from the vectors ξ of random numbers are changed. For the lowest value of Θ we have $n_\xi = n_{\xi,\text{min}}$, for the largest $n_\xi = n_{\xi,\text{max}}$, for the others in between. The total number of MCMC steps in the large-deviation simulation was always larger than the given values t_{id} , the actual values depending on the value of Θ and on the available computing time on the computing cluster, respectively. The longest running time occurred for the unfolding (forward) process $T = 1$, $n_{\text{MC}} = 8$ and took $t_{\text{id}} = 14.5 \times 10^8$ steps.

The results look similar to the 8 sweeps case, but the distributions are located a bit closer to each other here, such that the intersections of $P(W)$ and $P_{\text{rev}}(-W)$ occur at higher probability. In the inset of Fig. 6 the corresponding rescaled distribution for the reverse process is shown. Also for 16 MC sweeps a good agreement with the distribution for the forward process is visible, over more than 20 decades.

In Figs. 7 and 8 the corresponding results for the lower temperature $T = 0.3$ are shown. Again, Crooks theorem is confirmed with high precision, where here the distribution was even obtained down to probabilities as small

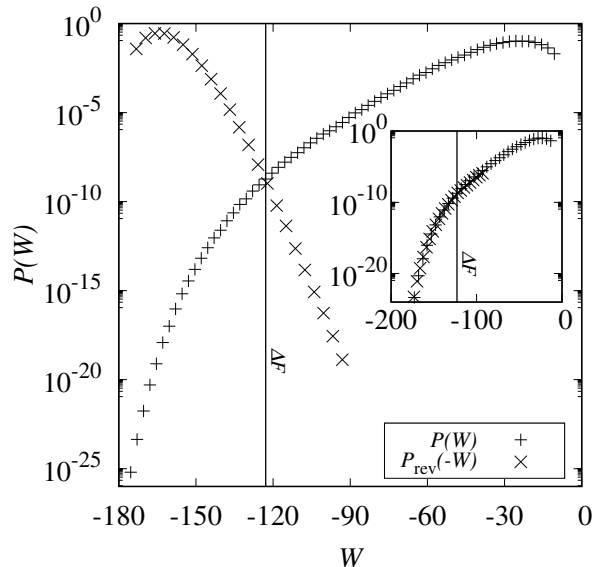


FIG. 6. Plain and mirrored work distributions for $T = 1$ and 16 sweeps of the forward and reverse process, respectively. They intersect near $W = \Delta F$, which is the exact value and indicated by the vertical line. The inset shows the same plot but with the distribution for the reverse process (cross symbols) rescaled as $P_{\text{rev}}(W) \exp(-(\Delta F - W)/T)$, according to the equation of Crooks, yielding a good agreement with $P(W)$.

as 10^{-46} .

Jarzynski Integrand

The integrand of $\langle e^{-W/T} \rangle = \int dW P(W) e^{-W/T}$ is shown in Fig. 9, for $T = 1$, $n_{\text{MC}} = 8$ and forward and reverse work processes, respectively. The point where the integrand peaks is exponentially relevant and can be used to approximate the integral. This, together with its probability, determines according to Jarzynski's equation the free energy difference.

Overlap

For two secondary structures \mathcal{S} and \mathcal{S}' and the equivalent notations $\{s(i)\}$ and $\{s'(i)\}$ for the pairing partners of the residues (0 if not paired), we define the *overlap*

$$\sigma(\mathcal{S}, \mathcal{S}') = \frac{1}{L} \sum_{i=1}^L \delta_{s(i), s'(i)} \quad (9)$$

where the Kronecker delta is given by $\delta_{k,l} = 1$ if $k = l$ and $\delta_{k,l} = 0$ else. Thus, the overlap equals one when $\mathcal{S}, \mathcal{S}'$

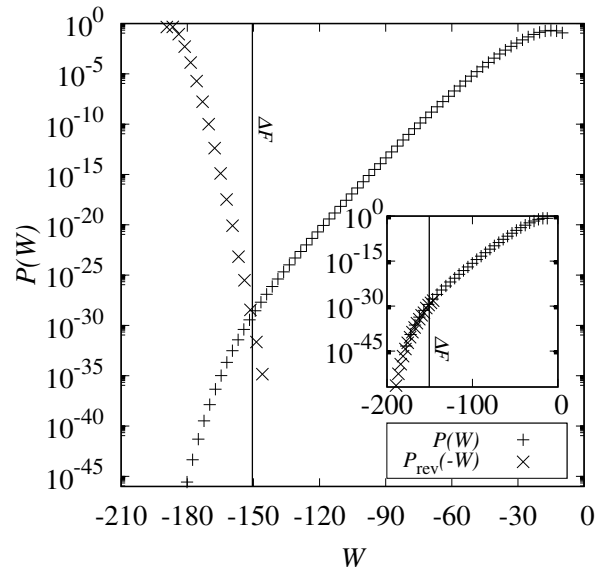


FIG. 7. Plain and mirrored work distributions for $T = 0.3$ and 8 sweeps of the forward and reverse process, respectively. They intersect near $W = \Delta F$, which is the exact value and indicated by the vertical line. The inset shows the same plot but with the distribution for the reverse process (cross symbols) rescaled as $P_{\text{rev}}(W) \exp(-(\Delta F - W)/T)$, according to the equation of Crooks, yielding a good agreement with $P(W)$.

denote the same secondary structure, and zero when they are completely different.

Force-extension curves

In addition to the overlap profiles $\sigma(f)$ we have presented in the main paper, we also used force extension curves (FECs) $n(f)$ to compare processes for equilibrium and non-equilibrium situations. Note that the extension $n(\mathcal{S})$ of a structure can be very much influenced by single base pairs. Thus two processes, which look very similar on the level of secondary structures, can be very different with respect to force-extension curves.

Samples for equilibrium and non-equilibrium FECs for forward processes, along with corresponding averages, are shown in Fig. 10. For the equilibrium case, a sigmoidal form can be observed, with some fluctuations, with a strong change near the critical force value where the folding-unfolding transition takes place [25]. For the non-equilibrium case, the typical FECs, i.e., with typical work values W far from ΔF , agree only for small values of f , i.e., in the initial phase of the process. On the other hand, the rare processes with W close to ΔF , where five different examples are shown here, are much more similar to the equilibrium FECs. Here, differences appear

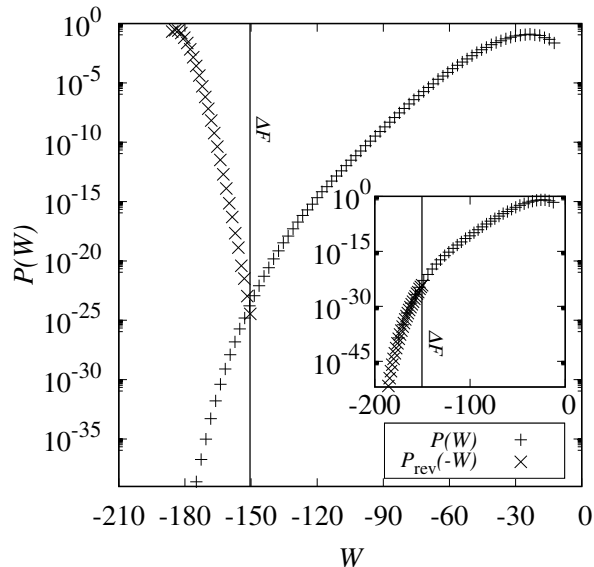


FIG. 8. Plain and mirrored work distributions for $T = 0.3$ and 16 sweeps of the forward and reverse process, respectively. They intersect near $W = \Delta F$, which is the exact value and indicated by the vertical line. The inset shows the same plot but with the distribution for the reverse process (cross symbols) rescaled as $P_{\text{rev}}(W) \exp(-(\Delta F - W)/T)$, according to the equation of Crooks, yielding a good agreement with $P(W)$.

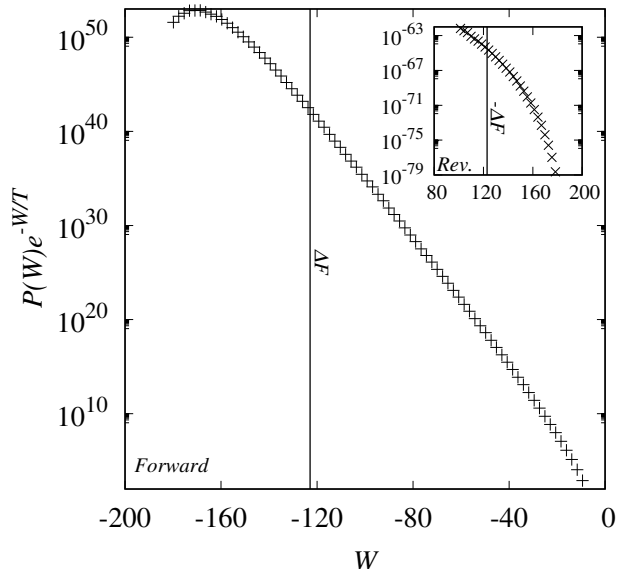


FIG. 9. Jarzynski integrand of the forward process for 8 sweeps at $T = 1$. Inset: Same for the reverse process, in which the maximum is not reached. Error bars are smaller than symbol sizes.

mainly near the critical folding-unfolding force.

Samples for equilibrium and non-equilibrium FECs for backward processes, along with corresponding averages, are shown in Fig. 11. The results correspond to the forward case, but the processes with *typical* values of W agree well with the average equilibrium FEC only for large values of f but not for small values of f . But this means they also agree in the initial phase of the process, before the critical folding-unfolding force value is reached. The FECs for work values $W \approx \Delta F$ are also for reverse processes much more similar to the equilibrium case than typical reverse processes.

These results are confirmed by averaging the absolute value of the differences between one FEC $n(f)$ and the mean equilibrium FEC $\bar{n}_{Eq}(f)$ over all available values of the force f , i.e., calculating $I^n = [\frac{1}{n_f} \sum_f |n(f) - \bar{n}_{Eq}(f)|]$ where the average [...] is over different realisations of $n(f)$. Even when considering equilibrium FECs for $n(f)$, respectively, there is some variation reflected by a non-zero average value I_0 . When using non-equilibrium FECs, with a specified binned value of W , one sees stronger differences, as visible in Fig. 12. Similar to I^σ , the closest agreements between non-equilibrium and equilibrium are seen near $W \approx \Delta F$. In contrast to I^σ the level of the equilibrium fluctuations is not reached for

the measurable quantity FEC.

-
- [1] C. Jarzynski, Phys. Rev. Lett. **78**, 2690 (1997).
 - [2] G. E. Crooks, J. Stat. Phys. **90**, 1481 (1998).
 - [3] J. Kurchan, JSTAT **2007**, P07005 (2007).
 - [4] U. Seifert, Eur. Phys. J. B **64**, 423 (2008).
 - [5] E. M. Sevick, R. Prabhakar, S. R. Williams, and D. J. Searles, Ann. Rev. Phys. Chem. **59**, 603 (2008).
 - [6] C. Jarzynski, Eur. Phys. J. B **64**, 331 (2008).
 - [7] M. Esposito, U. Harbola, and S. Mukamel, Rev. Mod. Phys. **81**, 1665 (2009).
 - [8] C. Jarzynski, Annual Review of Condensed Matter Physics **2**, 329 (2011).
 - [9] U. Seifert, Rep. Progr. Phys. **75** (2012), 10.1088/0034-4885/75/12/126001.
 - [10] R. Marsland III and J. England, Rep. Progr. Phys. **81** (2018), 10.1088/1361-6633/aa9101.
 - [11] A. K. Hartmann, *Big Practical Guide to Computer Simulations* (World Scientific, Singapore, 2015).
 - [12] G. Hummer and A. Szabo, Proc. Natl. Acad. Sci. **107**, 21441–21446 (2010).
 - [13] D. J. Evans, E. G. D. Cohen, and G. P. Morriss, Phys. Rev. Lett. **71**, 2401 (1993).
 - [14] D. J. Evans and D. J. Searles, Phys. Rev. E **50**, 1645 (1994).
 - [15] G. Gallavotti and E. G. D. Cohen, Phys. Rev. Lett. **74**, 2694 (1995).
 - [16] G. Gallavotti and E. G. D. Cohen, J. Stat. Phys. **80**, 931 (1995).
 - [17] J. Kurchan, J. Phys. A: Math. Gen. **31**, 3719 (1998).

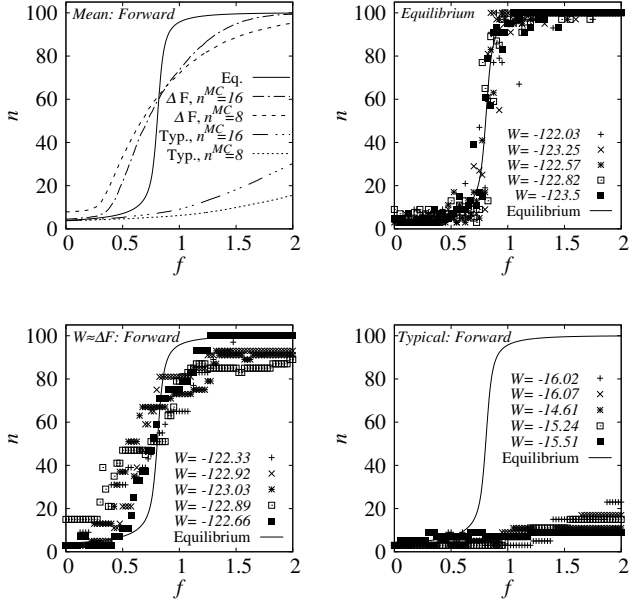


FIG. 10. Top left: Mean FECs, in equilibrium, for typical forward processes and for work values near ΔF , for two different number of n_{MC} of sweeps at $T = 1$. Top right: Samples of such single FECs in equilibrium. Bottom left: samples of non-equilibrium FECs with $n_{MC} = 8$ for W near ΔF . Bottom right: samples of typical non-equilibrium FECs, i.e., where $W \gg \Delta F$, with $n_{MC} = 8$. The solid line represents always the mean equilibrium FEC.

- [18] J. L. Lebowitz and H. Spohn, *J. Stat. Phys.* **95**, 333 (1999).
 [19] C. Maes, *J. Stat. Phys.* **95**, 367 (1999).
 [20] G. E. Crooks, *Phys. Rev. E* **60**, 2721 (1999).
 [21] G. E. Crooks, *Phys. Rev. E* **61**, 2361 (2000).
 [22] A. B. Adib, *Phys. Rev. E* **71**, 056128 (2005).
 [23] C. Jarzynski, *Phys. Rev. E* **56**, 5018 (1997).
 [24] G. Hummer and A. Szabo, *Proc. Nat. Acad. Sci.* **98**, 3658 (2001).
 [25] M. Müller, F. Krzakala, and M. Mézard, *Eur. Phys. J. E* **9**, 67–77 (2002).
 [26] A. K. Hartmann, *Phys. Rev. E* **65**, 056102 (2002).
 [27] J. A. Bucklew, *Introduction to rare event simulation* (Springer-Verlag, New York, 2004).
 [28] C. Dellago, P. G. Bolhuis, F. S. Csajka, and D. Chandler, *J. Chem. Phys.* **108**, 1964 (1998).
 [29] P. G. Bolhuis, D. Chandler, C. Dellago, and P. L. Geissler, *Ann. Rev. Phys. Chem.* **53**, 291 (2002), pMID: 11972010.
 [30] C. Giardinà, J. Kurchan, and L. Peliti, *Phys. Rev. Lett.* **96**, 120603 (2006).
 [31] V. Lecomte and J. Tailleur, *JSTAT* **2007**, P03004 (2007).
 [32] W. Staffeldt and A. K. Hartmann, *Phys. Rev. E* **100**, 062301 (2019).
 [33] A. K. Hartmann, P. L. Doussal, S. N. Majumdar,

A. Rosso, and G. Schehr, *Europhys. Lett.* **121**, 67004 (2018).

- [34] A. K. Hartmann, *Phys. Rev. E* **89**, 052103 (2014).
 [35] P. G. Higgs, *Phys. Rev. Lett.* **76**, 704 (1996).
 [36] B. Burghardt and A. K. Hartmann, *Phys. Rev. E* **71**, 021913 (2005).
 [37] R. Lorenz, S. H. Bernhart, C. Höner zu Siederdisen, H. Tafer, C. Flamm, P. F. Stadler, and I. L. Hofacker, *Algor. Mol. Biol.* **6**, 26 (2011).
 [38] U. Gerland, R. Bundschuh, and H. T., *Biophys. J.* **81**, 1324 (2001).
 [39] R. Nussinov, G. Pieczenik, J. R. Griggs, and D. J. Kleitman, *SIAM J. Appl. Math.* **35**, 68 (1978).
 [40] M. Mézard, G. Parisi, and M. Virasoro, *Spin glass theory and beyond* (World Scientific, Singapore, 1987).
 [41] I. Tinoco and C. Bustamante, *J. Mol. Biol.* **293**, 271 (1999).
 [42] G. E. Crooks and D. Chandler, *Phys. Rev. E* **64**, 026109 (2001).
 [43] C. Flamm, W. Fontana, I. L. Hofacker, and P. Schuster, *RNA* **6**, 325–338 (2000).
 [44] E. E. Dykeman, *Nucleic Acids Research* **43**, 5708–5715 (2015).
 [45] K. Darty, A. Denise, and Y. Ponty, *Bioinformatics* **25**, 1974 (2009).

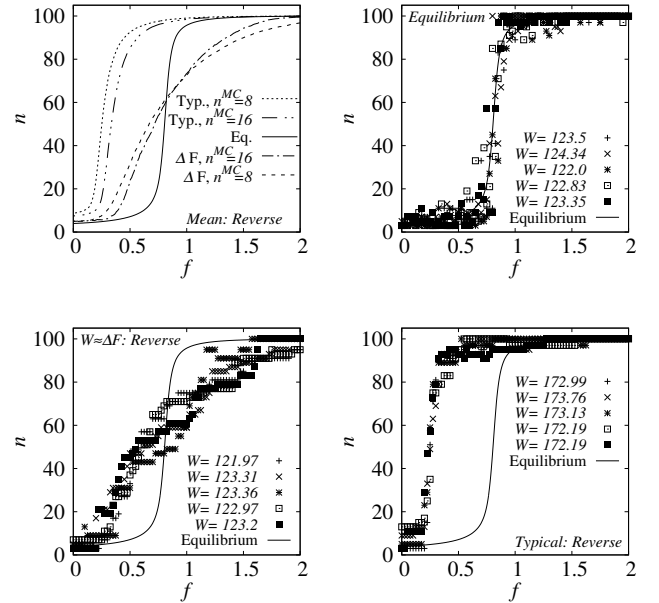


FIG. 11. Top left: Mean FECs, in equilibrium, for typical reverse processes and for work values near ΔF , for two different number of n_{MC} of sweeps at $T = 1$. Top right: Samples of such single FECs in equilibrium. Bottom left: samples of non-equilibrium reverse FECs with $n_{MC} = 8$ for W near ΔF . Bottom right: samples of typical non-equilibrium reverse FECs, i.e., where $W \gg \Delta F$, with $n_{MC} = 8$. The solid line represents always the mean equilibrium FEC.

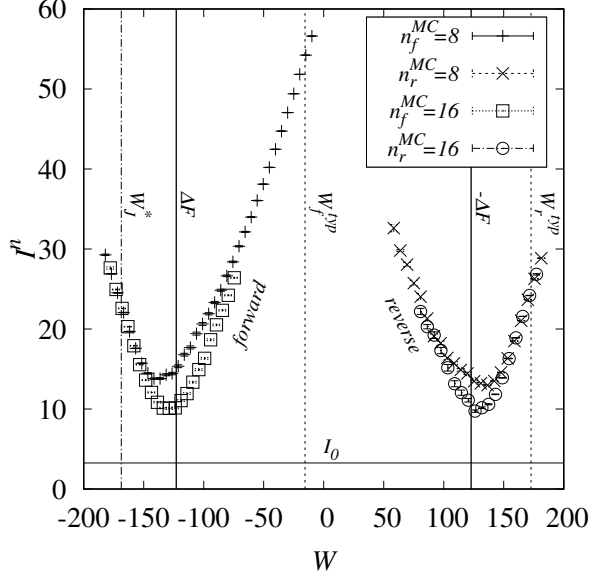


FIG. 12. Integrated extension difference I^n between equilibrium and non-equilibrium at $T = 1$. For 8 sweeps the entire work range is plotted, where for 16 sweeps only a range around the minimum is shown, for better visibility. I_0 , represented by a horizontal line, is the averaged value of I^n when comparing always two equilibrium FECs. The left curves represent the forward, the right ones the reverse process. Vertical lines indicate work values at (from left to right) the maximum W_J^* of the Jarzynski integrand, the free energy difference ΔF , the maximum W_f^{typ} of the forward process work distribution, the negative free energy difference $-\Delta F$ and the maximum point W_r^{typ} of the reverse process work distribution.